Letter

Search for the Sagittarius tidal stream of axion dark matter around 4.55 μeV

Andrew K. Yi,[1,2] Saebyeok Ahn,[1,2] Çağlar Kutlu,[1,2] JinMyeong Kim,[1,2] Byeong Rok Ko,[2,*] Boris I. Ivanov,[2] HeeSu Byun,[2] Arjan F. van Loo,[3,4] SeongTae Park,[2] Junu Jeong,[2] Ohjoon Kwon,[2] Yasunobu Nakamura,[3,4] Sergey V. Uchaikin,[2] Jihoon Choi,[2,†] Soohyung Lee,[2] MyeongJae Lee,[2,‡] Yun Chang Shin,[2] Jinsu Kim,[1,2] Doyu Lee,[2,§] Danho Ahn,[1,2] SungJae Bae,[1,2] Jiwon Lee,[1,2] Younggeun Kim,[2] Violeta Gkika,[2] Ki Woong Lee,[2] Seonjeong Oh,[2] Taehyeon Seong,[2] DongMin Kim,[2] Woohyun Chung,[2] Andrei Matlashov,[2] SungWoo Youn,[2] and Yannis K. Semertzidis[2,1]

[1]*Department of Physics, Korea Advanced Institute of Science and Technology, Daejeon 34141, Republic of Korea*

[2]*Center for Axion and Precision Physics Research, Institute for Basic Science, Daejeon 34051, Republic of Korea*

[3]*RIKEN Center for Quantum Computing (RQC), Wako, Saitama 351-0198, Japan*

[4]*Department of Applied Physics, Graduate School of Engineering, The University of Tokyo, Bunkyo-ku, Tokyo 113-8656, Japan*

(Received 2 February 2023; revised 13 April 2023; accepted 13 July 2023; published 24 July 2023)

We report the first search for the Sagittarius tidal stream of axion dark matter around 4.55 μeV using CAPP-12 TB haloscope data acquired in March of 2022. Our result excluded the Sagittarius tidal stream of Dine-Fischler-Srednicki-Zhitnitskii and Kim-Shifman-Vainshtein-Zakharov axion dark matter densities of $\rho_a \gtrsim 0.184$ and $\gtrsim 0.025$ GeV/cm^3, respectively, over a mass range from 4.51 to 4.59 μeV at a 90% confidence level.

DOI: 10.1103/PhysRevD.108.L021304

Approximately 85% of matter in our Universe consists of cold dark matter (CDM) according to the standard model of big bang cosmology and precision cosmological measurements [1]. Despite the strong evidence of the existence of dark matter [2], its nature remains unknown to date and falls into a category that is beyond the standard model of particle physics (SM). One of the strongest CDM candidates is the axion [3], which results from the breakdown of a new form of global symmetry introduced by Peccei and Quinn [4] to solve the strong *CP* problem in the SM [5]. The axion is predicted to be massive, abundant, and nonrelativistic and interacts very weakly with the SM [6].

A direct axion detection method by Sikivie [7], also known as the axion haloscope, uses the axion-photon coupling $g_{a\gamma\gamma} = \frac{\alpha g_\gamma}{\pi f_a}$, where α is the fine structure constant, g_γ is a model-dependent coupling constant, and f_a is the axion decay constant. The Kim-Shifman-Vainshtein-Zakharov (KSVZ) model [8] and the Dine-Fischler-Srednicki-Zhitnitskii (DFSZ) model [9] predict the $g_{a\gamma\gamma}$ with $g_\gamma = -0.97$ and 0.36, respectively. Thanks to the resonant conversion of axions to photons in a microwave cavity, the axion haloscope provides the most sensitive axion dark matter search via $g_{a\gamma\gamma}$ in the microwave region.

On the assumption that axions contribute to 100% of the local dark matter density and their signal shape follows the blue dashed line in Fig. 1(a) according to the standard halo model (SHM) [10], the CAPP-12 TB experiment recently collected data sensitive to DFSZ axion dark matter, whose mass is around 4.55 μeV [11]. Complementary to the SHM, dark matter of a tidal stream from the Sagittarius dwarf galaxy would have a velocity v of about 300 km/s and a velocity dispersion δv of about 20 km/s in our Solar System [12]. Only the 4096-bin search in Ref. [13] corresponds to a search for the Sagittarius tidal stream of axion dark matter to date. Another dark matter stream referred to as the "big flow" would possess $v \simeq 480$ km/s and $\delta v \lesssim 53$ m/s [14], and the relevant experimental searches can be found in Refs. [13,15,16]. For dark matter around 4.55 μeV, the signal widths from the Sagittarius tidal flow and the big flow would be $\simeq$150 and $\lesssim$0.62 Hz, respectively. The former fits the black solid line in Fig. 1(a), while the latter is much less than the frequency resolution bandwidth (RBW) $\Delta f = 10$ Hz of the CAPP-12 TB data

*Corresponding author.
brko@ibs.re.kr

†Also at Korea Astronomy and Space Science Institute, Daejeon 34055, Republic of Korea.

‡Also at Department of Physics, Sungkyunkwan University, Suwon 16419, Republic of Korea.

§Also at Samsung Electronics, Gyeonggi-do 16677, Republic of Korea.

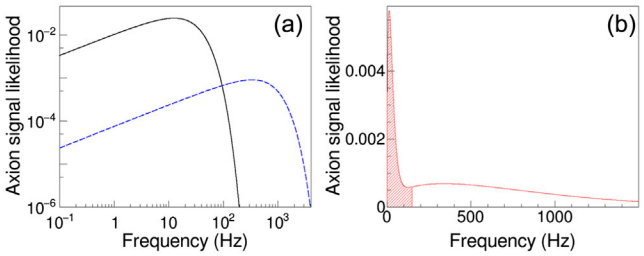

FIG. 1. Axion signal shapes for a corresponding frequency of 1.1 GHz following the SHM [blue dashed line in (a)] and the Sagittarius tidal stream model [black solid line in (a)]. The red solid line in (b) is the dark matter shape considered in this work assuming axion dark matter makes up 100% of the local dark matter density, where the Sagittarius tidal stream model and the SHM contribute 23% and 77%, respectively, and only the red hatched region corresponds to the signal model.

acquired in March of 2022 [11]. Considering such signal widths and $\Delta f = 10$ Hz, this search seeks dark matter of the tidal stream [12] around 4.55 μeV for the first time, utilizing the same data for our previous work [11]. This collateral search without a dedicated rescan is complementary to our recent SHM search [11].

The experimental parameters of the CAPP-12 TB haloscope can be represented by the expected axion signal power given in Eq. (1) and the schematic shown in Fig. 2, where Eq. (1) is valid when the axion mass m_a matches the frequency of the cavity mode ν ($m_a = h\nu/c^2$) and the cavity mode coupling to the receiver is 2:

$$P_a^{a\gamma\gamma} = 5.69\ \text{yW}\left(\frac{g_\gamma}{0.36}\right)^2\left(\frac{B_{\text{rms}}}{10.31\ \text{T}}\right)^2 \times \left(\frac{V}{36.85\ \text{L}}\right)\left(\frac{C}{0.6}\right)\left(\frac{Q_L}{35000}\right) \times \left(\frac{\nu}{1.1\ \text{GHz}}\right)\left(\frac{\rho_a}{0.114\ \text{GeV/cm}^3}\right). \quad (1)$$

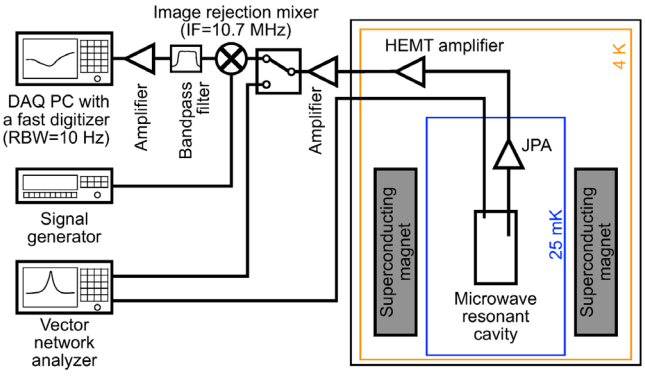

FIG. 2. Schematic of the CAPP-12 TB experiment, where HEMT and IF stand for high-electron-mobility transistor and intermediate frequency, respectively.

Equation (1) also uses the experimental parameters achieved by the CAPP-12 TB experiment which are the rms magnetic field over a cavity volume B_{rms} of 10.31 T, a cavity volume V of 36.85 L, a cavity-mode-dependent form factor C [17] of 0.6, and a loaded quality factor of the cavity mode Q_L of 35 000. Assuming axion dark matter makes up 100% of the local dark matter, where the Sagittarius tidal stream model and the SHM contribute 23% and 77% [12], respectively, the detected signal power of DFSZ axion dark matter of the tidal stream with the SHM contribution denoted as the red hatched in Fig. 1(b) is then expected to be 5.69 yW for the axion frequency of 1.1 GHz. This mixed signal is also similar to that in Ref. [18] and its power can be obtained by plugging in $\rho_a = 0.114\ \text{GeV/cm}^3$ in Eq. (1), which is the model considered in this work. Figure 2 not only shows the signal line from the cavity to the fast data acquisition (DAQ) system [19], but also another key experimental parameter, the 25 mK physical temperature of both the cavity and the Josephson parametric amplifier (JPA). The fast digitizer and the signal generator used an external reference clock [20] to set the frequencies.

The overall operation of the CAPP-12 TB experiment and the relevant measurements can be found in the literature [11]. Here, we describe the achieved crucial experimental parameters [11] in addition to those shown in Eq. (1) and Fig. 2. The JPA used by CAPP-12 TB [21,22] provided gains and noise temperatures of about 17 dB and 60 mK, respectively, at the target frequencies over the search range, where the target frequency is the central frequency of each individual power spectrum and ν was tuned to it. The gains and noise temperatures of the receiver chain other than the JPA were about 104 dB and 1.2 K, respectively. The total gains of the receiver chain were close to 121 dB around ν. The total gain in the measured power was removed to obtain the total system noise temperature T_n from the cavity and the receiver chain. The gain corrected power of each power spectrum was then parametrized using a Savitzky-Golay (SG) filter [23], and the extracted T_n around ν was approximately 215 mK as a roughly Lorentzian peak [11].

For each frequency step, we took 40 power spectra, with each being the average of 128 individual spectra [19]. Individual spectra with an analysis frequency span of 150 kHz were measured over a 0.1 s interval; hence, $\Delta f = 10$ Hz, as mentioned above, and the integrated time Δt for the measurement of the power at each frequency P_{f_i} was 512 s. During this DAQ duration of 512 s, ν drifts with a spread of about 290 Hz due to our experimental imperfections, while the axion signal shape is almost invariant under Earth motions as explained below. As our cavity bandwidth is about 31 kHz for ν around 1.1 GHz, the axion signal power at ν and that at 290 Hz away from ν differ by less than 0.1% in the case of ν drift, which is negligible to our result.

The 150 kHz analysis span and our frequency tuning steps of 10 kHz create 15 power spectra overlaps in most of

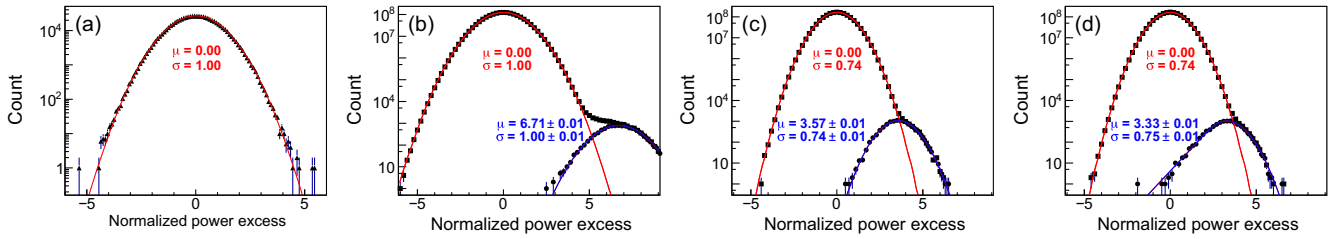

FIG. 3. Triangles in (a) show the normalized power excess distribution of the normalized grand power spectrum from the CAPP-12 TB data after applying a frequency-independent scale factor of 0.74. (b)–(d) show the normalized power excess distributions of 10 000 normalized grand power spectra from the 10 000 simulated CAPP-12 TB experiments. Rectangles in (b)–(d) are from all frequencies of the normalized grand spectra, while the circles there are from the frequency with the simulated axion signals. (b) and (c) were obtained without a filtering procedure, while (d) was obtained with filtering. (b) was obtained after background subtraction with a perfect fit, while (c) and (d) were obtained with our SG filter with $d = 4$ and $W = 37$. Lines are a Gaussian fit resulting in μ (mean) and σ (width), except for the Crystal Ball line shape [27] fit to the circle distribution in (d).

the frequency range, meaning that the total Δt for the P_{f_i} measurement is at least 7680 s. During the P_{f_i} measurement time of 10 000 s considering the cavity tuning and the relevant measurements conservatively, the rotational and orbital motions of Earth with corresponding speeds of 0.4 and 30 km/s can shift the signal frequency at most by about 1.07 and 0.22 Hz, respectively. Hence, the signal broadening caused by the motions of Earth are negligible compared to the RBW of 10 Hz and to the expected signal width of about 150 Hz.

Given that the signal frequency shifts are much less than the RBW of 10 Hz for the duration of the P_{f_i} measurement, P_{f_i} can be calculated as the weighted average of the powers measured from all spectra having that frequency, which allows us to use, without a further RBW reduction process, the similar analysis procedure for the axion dark matter search of the SHM [24–26]. Owing to the absence of a dedicated rescan schedule, our analysis strategy here seeks to let the most significant power excess have significance under a certain threshold value and as small as possible. Having a narrower signal window and lower ρ_a, the signal-to-noise ratio (SNR) is naïvely expected to be consistent approximately with that in our previous work [11]. If a threshold of 3.718 of the normalized power excess to get a one-side 90% upper limit corresponding to the expected SNR of 5 would be applicable without rescanning, we could expect a search sensitive to the Sagittarius tidal stream of DFSZ axion dark matter considered in this study at a 90% confidence level (CL).

First, we applied a similar filtering procedure in Ref. [25] to remove narrow spikes in each power spectrum. Each power spectrum was parametrized via SG smoothing with a polynomial of degree 4 ($d = 4$) in a 75-point window ($2W + 1 = 75$) at $\Delta f = 10$ Hz for both the filtering (see the details in Appendix A) and background subtraction thereafter, where the 75-point window corresponds to 5 times the signal window used for this search. We found that the normalized power excess obtained right after background subtraction from each power spectrum follows a Gaussian distribution whose width is not 1, but 0.97. This narrower Gaussian width resulted from the SG filter parameters of $d = 4$ and $W = 37$ used in this work, because we found no such bias for SG parameters of $d = 4$ and $W = 1000$ used in our previous work [11]. Our simulation data explained below also predict the bias induced from the SG filter with $d = 4$ and $W = 37$, and thus a possible systematic effect is discussed there as well. After filtering and background subtraction, all of the power spectra were combined as a single power spectrum. We then summed three nonoverlapping spectral lines so that $\Delta f = 30$ Hz, and this spectrum is referred to as the "combined power spectrum" (see the details in Appendix B). This RBW reduction to 30 Hz ensures a smaller threshold value because it decreases the significance of power excess, albeit it was a compromise with the decrease in SNR that accompanies this process [11]. Our "grand power spectrum" was constructed from the combined power spectrum by coadding [24] five continuously adjacent 30 Hz power spectral lines. Each spectral line was weighted by the signal shape [25], which is indicated by the red hatched region in Fig. 1(b). Figure 3(a) shows the normalized power excess distribution from the grand power spectrum following the standard Gaussian after correcting for a frequency-independent scale factor of 0.74 to remove the known bias in power excess induced by background subtraction [26]. From such a standard Gaussian distribution, we found that the greatest significance of the power excess is less than 5.4 and thus were able to exclude all of the power excess by applying a threshold of 5.4 without rescanning. For the most significant power excess, we calculated the χ^2 probability to check the signal compatibility (see the details in Appendix C). From it, we concluded that the excess is not compatible with the signal model in this work and thus no dark matter of the tidal stream was found around 4.55 μeV.

We estimated the SNR efficiency and other possible systematic effects with 10 000 simulated CAPP-12 TB experiments with simulated axion signals at an arbitrary frequency within the search range. The input signal power

and shape of the simulated axion signals follow Eq. (1) and the red hatched region in Fig. 1(b), respectively. In order to avoid the aforementioned bias observed in the power excess immediately after background subtraction by the SG filter above, we instead used backgrounds parametrized by another SG filter with $d = 4$ and $W = 1000$ as our simulation inputs. Figures 3(b) and 3(c) show the distributions of the normalized power excess from 10 000 grand power spectra from the 10 000 simulated CAPP-12 TB experiments without the filtering procedure, where the former was obtained by background subtraction using the simulation inputs, i.e., a perfect fit, and the latter was obtained using the SG filter with $d = 4$ and $W = 37$. The rectangles in Figs. 3(c) and 3(d) show a width of 0.74, agreeing with the CAPP-12 TB data. The circles in Figs. 3(b) and 3(c) are from the frequency with the simulated axion signals. From these, we estimated that our background subtraction efficiency was about 72%. Figure 3(d) is identical to Fig. 3(c), but with the filtering procedure applied. The filtering efficiency was extracted and determined to be about 92% from the distributions of the circles in Figs. 3(c) and 3(d). A fast Fourier transform (FFT) returns discrete power lines only at the set frequencies and thus can be inefficient unless the input signal frequencies match those frequencies. The efficiency depends on the number of spectral lines with the signal power; e.g., it is at worst 40.5% for a single spectral line search [13]. For the search here with 15 spectral lines, the minimum efficiency was estimated to be about 97% for the 5 Hz offset between the input and the set frequencies, which included at most 0.1% inefficiency due to the RBW reduction from 10 to 30 Hz. Our total SNR efficiency is approximately 64% taking into account the three sources, 72% from background subtraction, 92% from narrow spike filtering, and 97% from FFT with maximum signal misalignment. Further frequency-dependent SNR degradation due to the additional line attenuation insensitive to our noise calibration [11] was also reflected in our exclusion limits.

The 10 000 simulated CAPP-12 TB experiments were also used to estimate a possible systematic effect that can come from the bias observed in the power excess right after background subtraction using our SG filter with $d = 4$ and $W = 37$. Using the large-statistic simulation data, we were able to separate the systematic effects from the statistical fluctuations by comparing the results with the perfect fit and our SG filter. The noise fluctuations resulting from the perfect fit follow the radiometer equation [28], whereas we found that those resulting from the SG filter do not. The additional contribution to the noise fluctuations resulting from the SG filter was extracted and found to be about 0.5% of the statistical fluctuations. The systematic uncertainty of 6% in the noise temperature measurement was dominant [11] and this factor was taken into account in our exclusion limits.

For $4.51 < m_a < 4.59$ μeV, we set the 90% upper limits of the densities of axion dark matter of the Sagittarius tidal stream [12], as shown in Fig. 4. Dark matter of the tidal streams was ruled out for densities of $\rho_a \gtrsim 0.184$ and $\gtrsim 0.025$ GeV/cm^3 for DFSZ and KSVZ axions, respectively, at a 90% CL over the search range. The exclusion limits for DFSZ axions are less sensitive than the aforementioned expected value of 0.114 GeV/cm^3, which resulted from the lower SNR efficiency and the larger threshold compared to our previous axion dark matter search of the SHM [11]. This was an inevitable side effect of reprocessing the data from Ref. [11] without additional scanning time. Nevertheless, our result excluded the Sagittarius tidal stream of KSVZ axion dark matter for the first time, down to about 5.6% of the local dark matter density assuming the dark matter model considered in this work [12].

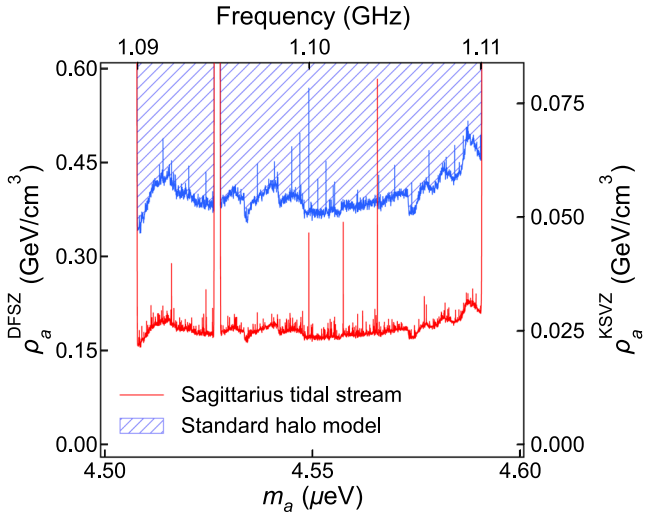

FIG. 4. Assuming axion dark matter makes up 100% of the local dark matter density, the blue hatched region shows the exclusion limits for the axion dark matter densities, ρ_a^{DFSZ} in left and ρ_a^{KSVZ} in right, at a 90% CL [11] and the red solid line shows those achieved by this work. The former used the SHM [10] contribution of 100% [blue dashed line in Fig. 1(a)] and the latter the Sagittarius tidal stream model and the SHM contributions of 23% and 77%, respectively [12], but only considering the red hatched region in Fig. 1(b). No results are available around an axion mass of 4.527 μeV due to mode crossing. The spikes are less sensitive frequency points with fewer statistics resulting from the filtering procedure mentioned in the text.

In summary, we report the first search for the Sagittarius tidal stream of axion dark matter around 4.55 μeV using CAPP-12 TB haloscope data acquired in March of 2022. We excluded the Sagittarius tidal stream of DFSZ and KSVZ axion dark matter densities of $\rho_a^{\mathrm{DFSZ}} \gtrsim 0.184$ GeV/cm^3 and $\rho_a^{\mathrm{KSVZ}} \gtrsim 0.025$ GeV/cm^3, respectively, over a mass range from 4.51 to 4.59 μeV at a 90% CL.

This work was supported by the Institute for Basic Science (IBS) under Project Code No. IBS-R017-D1-2023-a00 and Japan Science and Technology Agency ERATO

(Grant No. JPMJER 1601). A. F. v. L. was supported by a Japan Society for the Promotion of Science postdoctoral fellowship.

APPENDIX A: NARROW SPIKE FILTERING

As depicted in Fig. 5, the 40 power spectra taken at each tuning step were sampled into four groups and the ten power spectra in each group were averaged to result in four power spectra so that narrow spikes which may not show up in a single spectrum would do so after ten averages. In order to obtain a threshold value as small as possible, we applied tighter filtering conditions. Each of the four power spectra was fitted using the SG filter with $d = 4$ and $W = 37$ and the normalized power excesses over 3.5 were then removed in each of the four power spectra. A neighboring frequency point on both sides of the narrow spike passing the threshold 3.5 was also eliminated. After averaging the four power spectra, filtering was applied again to the averaged power spectrum using the same conditions described above.

APPENDIX B: COMBINED POWER SPECTRUM

Figure 6 illustrates the construction of the combined power spectrum. Each of the consecutive background-subtracted power spectra corresponds to a power excess shown in Fig. 5. All of them and the associated errors were rescaled by the expected total axion signal power, where the rescaling across the spectrum follows the cavity line shape reflecting the corresponding Q_L [11,25]. The excess at each frequency was then obtained as the weighted average of the excess from all the relevant individual spectra that are combined.

APPENDIX C: SIGNAL COMPATIBILITY TEST

We checked the signal compatibility by comparing the two signal shapes; one is from data and the other from the model considered in this work. Data points are red solid triangles with error bars in Fig. 7 from the combined power spectrum which retains the signal line shape. The simulation expectations including our signal model reflecting the significance of the excess observed from data are blue solid circles in Fig. 7. Our $\chi^2 = \sum_i \frac{(d_i - e_i)^2}{\sigma_{d_i}^2}$, where d_i and e_i are data and the expectations, respectively, and σ_{d_i} the d_i errors. Note that the σ_{d_i} are the rescaled errors after the background estimation from the fit shown as the red dashed line in Fig. 5, while the d_i and e_i are the rescaled power excesses after background subtraction by the fit. The χ^2 was built with five continuously neighboring excesses, where the frequency with the greatest significance was aligned with the second of the five excesses according to the signal shape, as denoted by the red hatched region in Fig. 1(b). The calculated χ^2 probability with a degree of freedom of 4 was about 1.8×10^{-9}, which implies the two signal shapes are not compatible with each other.

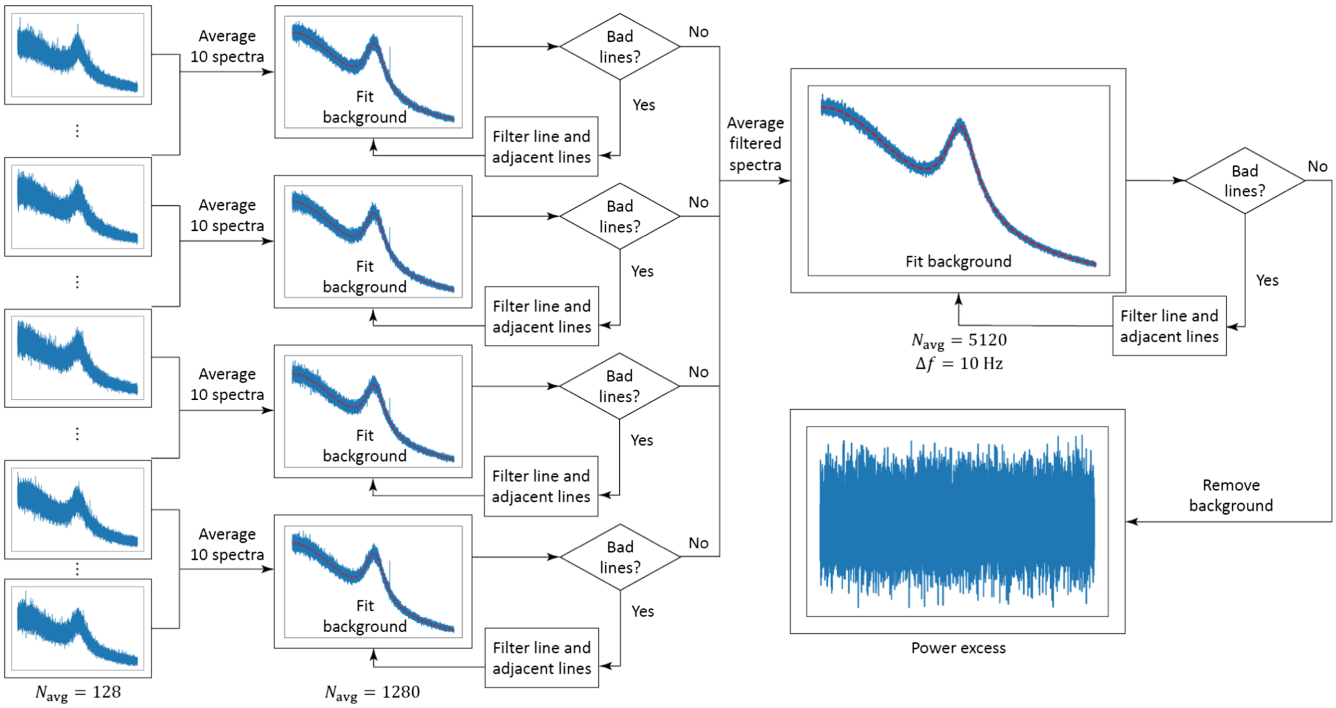

FIG. 5. Procedure of the narrow spike filtering. Red dashed lines show the background fits by our SG filter with $d = 4$ and $W = 37$.

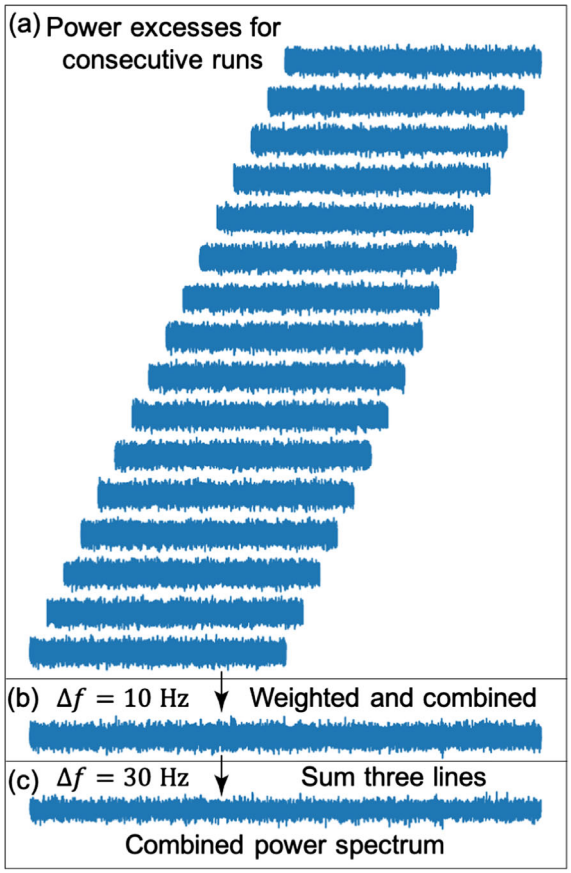

FIG. 6. Construction of the combined power spectrum. (a) shows the background-subtracted power spectra shown in Fig. 5 for consecutive frequency steps. (b) and (c) are the combined power spectrum with Δf of 10 and 30 Hz, respectively, where the excess at each frequency was obtained as the weighted average of the excess from all the relevant individual spectra shown in (a).

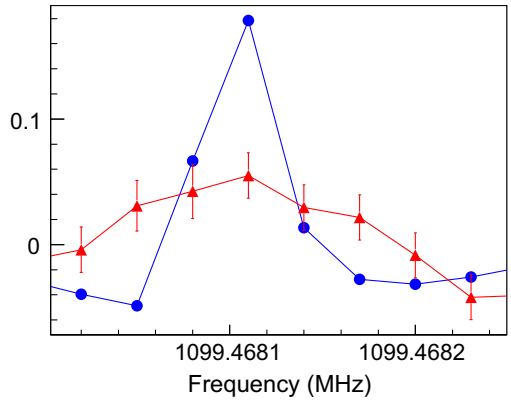

FIG. 7. Red solid triangles with error bars are data from the combined power spectrum and blue solid circles the simulation expectations. The signal compatibility was checked with five continuously neighboring excesses from the third to the seventh excess corresponding to the signal region. Note that the excesses and errors are dimensionless due to the rescaling mentioned in Appendix B and the negative excesses can be found due to background subtraction in the presence of axion signal, as also seen in Ref. [26].

[1] P. A. R. Ade *et al.* (Planck Collaboration), Astron. Astrophys. **594**, A13 (2016).
[2] V. Rubin and W. K. Ford, Jr., Astrophys. J. **159**, 379 (1970); Douglas Clowe, Maruša Bradač, Anthony H. Gonzalez, Maxim Markevitch, Scott W. Randall, Christine Jones, and Dennis Zaritsky, Astrophys. J. **648**, L109 (2006).
[3] S. Weinberg, Phys. Rev. Lett. **40**, 223 (1978); F. Wilczek, Phys. Rev. Lett. **40**, 279 (1978).
[4] R. D. Peccei and H. R. Quinn, Phys. Rev. Lett. **38**, 1440 (1977).
[5] G. 't Hooft, Phys. Rev. Lett. **37**, 8 (1976); Phys. Rev. D **14**, 3432 (1976); **18**, 2199(E) (1978); J. H. Smith, E. M. Purcell, and N. F. Ramsey, Phys. Rev. **108**, 120 (1957); W. B. Dress, P. D. Miller, J. M. Pendlebury, P. Perrin, and N. F. Ramsey, Phys. Rev. D **15**, 9 (1977); I. S. Altarev *et al.*, Nucl. Phys. **A341**, 269 (1980).
[6] J. Preskill, M. B. Wise, and F. Wilczek, Phys. Lett. **120B**, 127 (1983); L. F. Abbott and P. Sikivie, Phys. Lett. **120B**, 133 (1983); M. Dine and W. Fischler, Phys. Lett. **120B**, 137 (1983).
[7] P. Sikivie, Phys. Rev. Lett. **51**, 1415 (1983); Phys. Rev. D **32**, 2988 (1985).
[8] J. E. Kim, Phys. Rev. Lett. **43**, 103 (1979); M. A. Shifman, A. I. Vainshtein, and V. I. Zakharov, Nucl. Phys. **B166**, 493 (1980).
[9] A. R. Zhitnitskii, Yad. Fiz. **31**, 497 (1980) [Sov. J. Nucl. Phys. **31**, 260 (1980)]; M. Dine, W. Fischler, and M. Srednicki, Phys. Lett. **104B**, 199 (1981).

[10] Michael S. Turner, Phys. Rev. D **42**, 3572 (1990).
[11] Andrew K. Yi *et al.*, Phys. Rev. Lett. **130**, 071002 (2023).
[12] K. Freese, P. Gondolo, H. J. Newberg, and M. Lewis, Phys. Rev. Lett. **92**, 111301 (2004); K. Freese, P. Gondolo, and H. J. Newberg, Phys. Rev. D **71**, 043516 (2005).
[13] L. Duffy, P. Sikivie, D. B. Tanner, S. Asztalos, C. Hagmann, D. Kinion, L. J Rosenberg, K. van Bibber, D. Yu, and R. F. Bradley, Phys. Rev. Lett. **95**, 091304 (2005); Phys. Rev. D **74**, 012006 (2006).
[14] P. Sikivie, Phys. Lett. B **567**, 1 (2003).
[15] J. Hoskins *et al.*, Phys. Rev. D **84**, 121302(R) (2011).
[16] J. Hoskins *et al.*, Phys. Rev. D **94**, 082001 (2016).
[17] B. R. Ko, H. Themann, W. Jang, J. Choi, D. Kim, M. J. Lee, J. Lee, E. Won, and Y. K. Semertzidis, Phys. Rev. D **94**, 111702(R) (2016).
[18] Chris W. Purcell, Andrew R. Zentner, and Mei-Yu Wang, J. Cosmol. Astropart. Phys. 08 (2012) 027.
[19] S. Ahn, M. J. Lee, A. K. Yi, B. Yeo, B. R. Ko, and Y. K. Semertzidis, J. Instrum. **17**, P05025 (2022).
[20] FS725 Rubidium Frequency Standard, Stanford Research Systems, 1290-D Reamwood Avenue, Sunnyvale, CA 94089, USA.
[21] T. Yamamoto, K. Inomata, M. Watanabe, K. Matsuba, T. Miyazaki, W. D. Oliver, Y. Nakamura, and J. S. Tsai, Appl. Phys. Lett. **93**, 042510 (2008).
[22] Çağlar Kutlu, Arjan F. van Loo, Sergey V. Uchaikin, Andrei N. Matlashov, Doyu Lee, Seonjeong Oh, Jinsu Kim, Woohyun Chung, Yasunobu Nakamura, and Yannis K. Semertzidis, Supercond. Sci. Technol. **34**, 085013 (2021).
[23] A. Savitzky and M. J. E. Golay, Anal. Chem. **36**, 1627 (1964).
[24] S. J. Asztalos *et al.*, Phys. Rev. D **64**, 092003 (2001).
[25] B. M. Brubaker, L. Zhong, S. K. Lamoreaux, K. W. Lehnert, and K. A. van Bibber, Phys. Rev. D **96**, 123008 (2017).
[26] S. Ahn, S. Lee, J. Choi, B. R. Ko, and Y. K. Semertzidis, J. High Energy Phys. 04 (2021) 297.
[27] T. Skwarnicki, Ph.D. thesis, INP, Cracow, 1986.
[28] R. H. Dicke, Rev. Sci. Instrum. **17**, 268 (1946).